RSC Advances

RSC Publishing

PAPER

View Article Online
View Journal | View Issue

Sintered gold nanoparticles as an electrode material for paper-based electrochemical sensors†

Cite this: *RSC Advances*, 2013, **3**, 8683

Devi D. Liana,[ab] Burkhard Raguse,[a] Lech Wieczorek,[a] Geoff R. Baxter,[a] Kyloon Chuah,[b] J. Justin Gooding[bc] and Edith Chow*[a]

Received 8th January 2013,
Accepted 20th March 2013

DOI: 10.1039/c3ra00102d

www.rsc.org/advances

A simple and economical process for fabricating gold electrodes on paper is presented. Gold nanoparticles stabilised with 4-(dimethylamino)pyridine were applied to nail-polish coated filter paper and made conductive using a camera flash sintering step. To test the ability of the sintered gold nanoparticle film to function as a sensing platform, cysteine was self-assembled on gold and used for the electrochemical determination of copper ions. The cysteine-sintered gold nanoparticle film was able to successfully complex copper ions, with only minor differences in performance compared with a standard cysteine-modified solid-state gold disk electrode. Investigations by Raman spectroscopy revealed the successful removal of the 4-(dimethylamino)pyridine coating during sintering, whereas electrochemical impedance spectroscopy and scanning electron microscopy suggested that differences in the sensing performance could be attributed to the rougher morphology of the sintered gold nanoparticle electrode.

Introduction

Paper is highly suitable as a substrate for producing analytical sensors due to its versatility, disposability, abundance and low cost.[1–11] Martinez *et al.*[6,7] introduced the concept of microfluidic channels on paper for multianalyte colorimetric detection by confining the liquid sample within a specific region using a photoresist. Since then, many avenues for research on paper have been explored such as in paper-cut microfluidic devices[12] and 3D origami paper.[13–15] In order to develop a paper-based analytical sensor that can maintain the sensitivity and selectivity offered by traditional methods, yet be simple and cheap, electrochemical transduction methods are well-suited. Several groups have developed paper-based electrochemical sensors for environmental monitoring,[16–18] food monitoring[18,19] and clinical applications.[3,9,17] Lankelma *et al.*[18] recently developed a flow injection electrochemical analysis system consisting of a nitrocellulose sheet with one end in contact with an upper buffer reservoir and the other end in contact with a long filter paper strip immersed in a lower reservoir sink. Due to the gravity-driven capillary wicking solution, a continuous flow of buffer solution along the nitrocellulose sheet could be achieved. The utility of this design was investigated for detecting glucose from a urine sample with solid-state electrodes placed underneath the nitrocellulose sheet. The glucose oxidase was deposited on the downstream end of the platinum working electrode/nitrocellulose pad, allowing the oxidation of potentially interfering redox species to occur first upstream resulting in temporal and spatial resolution of the analyte and interfering species.

A more commonly adopted approach relies not on the use of solid-state electrodes placed in intimate contact with the paper but rather on the use of disposable screen-printed electrodes.[9,17] Dungchai *et al.*[9] fabricated paper-based microfluidic devices by screen printing carbon ink for the working and counter electrodes and silver/silver chloride ink for the reference electrode onto paper. The screen-printed electrodes were isolated from the contact pads with a photoresist and were used for the simultaneous determination of glucose, lactate and uric acid by spotting the working electrode with the appropriate enzyme. Nie *et al.*[17] also designed paper-based electrochemical sensors by screen-printing electrodes using carbon ink and silver/silver chloride ink together with microfluidic channels patterned by photolithography or wax printing. The electrode-patterned paper was combined with a second paper strip positioned across the electrodes to facilitate continuous wicking of the sample solution (glucose and heavy metal ions). Moreover, Nie *et al.*[19] screen-printed electrodes and combined them with a commercial hand-held glucometer as an electrochemical reader for glucose, cholesterol, and lactate.

The previously described approaches are all based on carbon working electrodes whereas the use of gold electrodes on paper is an unexplored area despite its potential for surface

[a]*CSIRO Materials Science and Engineering, PO Box 218, Lindfield, NSW 2070, Australia. E-mail: edith.chow@csiro.au*
[b]*School of Chemistry, The University of New South Wales, Sydney, NSW 2052, Australia*
[c]*Australian Centre for NanoMedicine, The University of New South Wales, Sydney, NSW 2052, Australia*

† Electronic supplementary information (ESI) available. See DOI: 10.1039/c3ra00102d

modification by thiols. Self-assembled monolayers (SAMs) of thiols on gold have been widely exploited in the past 20 years as a basis for electrochemical sensors.[20–22] Depending on the analyte of interest, the SAM can be tuned with different functionalities or receptor groups. These functionalities include amino acids and peptides,[23–25] crown ethers,[26] enzymes,[27–33] DNA,[34–36] carbon nanotubes,[37,38] dendrimers,[39,40] and nanoparticles[41] tethered directly onto the surface or *via* the modification of SAM building blocks.

Several challenges exist in the realisation of disposable gold electrodes on paper such as the cost involved with the utilisation of this precious metal and the fabrication of conductive gold electrode structures. These challenges can potentially be addressed through the formation of conductive thin films of gold nanoparticles using minimal quantities of gold nanoparticle ink.

In order to produce a conductive structure from gold nanoparticles deposited on a substrate, several techniques have been investigated based on the sintering of metallic nanoparticles such as microwave,[42] electrical,[43,44] laser,[45] infra-red[46] and light flash sintering.[47–53] The sintering process removes the organic stabilising molecules around the nanoparticles, resulting in coalescence of the nanoparticles and the formation of a highly conductive track. For example, the infrared sintering of gold nanoparticles on kaolin-coated paper[46] resulted in a volume resistivity decrease to 25 μΩ cm (*cf.* bulk gold resistivity 2.65 μΩ cm) whereas laser sintering (520 nm) of gold nanoparticles on a polymer substrate[45] resulted in a resistivity decrease to 5.41 μΩ cm.

The light flash sintering process is perhaps the simplest and fastest sintering technique and has the added advantage that it can be performed at room temperature. A pulsed xenon flash lamp (such as from a camera flash unit) is commonly used as the light emitted is broad spectrum (380 nm to 1 μm) and the sintering process can be performed within a few milliseconds. It has been observed that the absorption of light by the nanoparticles results in localised heating and removal of the protecting agent on the nanoparticles. Subsequently, necking connections are formed between the nanoparticles leading to a decrease in electrical resistance. Several factors have been known to contribute to the success of the sintering process such as irradiation energy, pulse number, pulse width and interval time between pulses.[48–50,53]

Despite the attractiveness of sintering gold nanoparticles, they have yet to be utilised for electrochemical sensor fabrication. Here, we demonstrate the potential of using sintered gold nanoparticles as a working electrode *via* the deposition of gold nanoparticles onto paper and subsequent camera flash sintering. As a model system, the self-assembly of cysteine on the sintered gold nanoparticles was investigated and the electrochemical sensing performance was evaluated for Cu^{2+} ions. The viability of gold nanoparticles as a route for gold electrodes could allow for disposable, low-cost sensing in a range of application areas.

Experimental methods

Chemical & apparatus

All chemicals were of analytical grade, used as received unless otherwise stated, and were purchased from Sigma Aldrich (Sydney, Australia): ethyl methyl ketone, ammonium acetate, copper(II) sulphate, L-cysteine, sodium chloride, ethylenediaminetetraacetic acid (EDTA), potassium ferricyanide, tetraoctylammonium bromide (TOAB), toluene, sodium borohydrate, sodium carbonate, hydrogen tetracholoaurate, dimethylamino pyridine (DMAP), sodium nitrate, nitric acid, sodium hydroxide and potassium hydroxide.

All solutions were prepared in Milli-Q water (>18.2 MΩ cm from Millipore) unless otherwise stated. Glassware used in the experiment were rinsed thoroughly with 6 M nitric acid and then with Milli-Q water to remove trace metals. The buffer solution used in this work was 50 mM ammonium acetate (pH 7.0) with the pH value adjusted with either sodium hydroxide or nitric acid solutions. A stock copper solution (0.1 M) was prepared in Milli-Q water and dilute copper solutions were prepared by serial dilution of the stock solution in ammonium acetate buffer. Copper concentrations were verified by inductively coupled plasma-mass spectrometry and are reported herein.

A screen-printing kit was purchased from Nehoc, Australia. Carbon ink (C-774) and silver/silver chloride ink (AGCL-675 C) were purchased from Conductive Compounds, New Hampshire, United States. Whatman® filter paper (No. 1, 60 × 60 cm) was obtained from Sigma Aldrich. Nail polish (satin sheet, Face of Australia) was purchased from Priceline, (Sydney, Australia). A calligraphy pen (width 0.2 cm, Automatic Pen No. 1) was purchased from Will's Quills (Sydney, Australia). Polycrystalline gold disk working electrodes (diameter 1 mm) and silver/silver chloride reference electrodes were from eDAQ and the platinum wire counter electrode was from Goodfellow (Huntingdon, United Kingdom).

Synthesis of gold nanoparticles coated with DMAP

Gold nanoparticles were synthesised following the Brust method[41] and transferred to the aqueous phase containing DMAP following the method by Gittins and Caruso.[54] Briefly, a solution of $HAuCl_4$ was added to a stirred solution of TOAB in toluene. Stirring was continued for 10 min and then followed by the addition of sodium borohydride, which resulted in reduction of the gold. After 2 h, the lower aqueous phase was removed and the toluene phase was subsequently washed twice with sulfuric acid, twice with sodium carbonate and twice with water. For the phase transfer of the nanoparticles from the organic to the aqueous phase, an aqueous solution of DMAP was added to the as-prepared nanoparticles. The solution containing the DMAP-gold nanoparticles was then separated and evaporated under a gentle stream of nitrogen leaving gold nanoparticle powder. The dried DMAP-gold nanoparticle powder was stored at 4 °C and DMAP-gold nanoparticle ink solution was prepared as required (1% w/v in 50% ethanol). All ink solutions were filtered with a 0.22 μm Millex® GS filter unit (Millipore, Australia) prior to use. The size of the DMAP-gold nanoparticles was determined using

dynamic light scattering (High Performance Particle Sizer, Malvern Instruments, Worcestershire, UK) to be 6 ± 2 nm.

Fabrication of paper-based sensor modified with cysteine

First a hydrophobic barrier was formed on the filter paper (Whatman® No. 1) to confine the solution in the region containing the working, reference and counter electrodes and to isolate the solution from the connection pads. A Xerox Phaser 8560N solid ink wax printer (Fuji Xerox, Australia) was used to print the hydrophobic wax barrier, which was designed in Adobe Photoshop 6 software.[55,56] The hydrophobic barrier pattern was designed in Adobe Photoshop 6 software. After printing the wax (width 0.5 cm) on paper, it was cooled and solidified without further spreading. The wax was then melted using a laminator (H220 High Speed from GBC, Australia) with a setting of 2 × 125 Mic. The printed paper was then placed between two transparency sheets and passed one to six times through the laminator.

In order to avoid non-specific binding of cysteine to the counter and reference electrodes, the paper-based electrochemical sensor was designed as a "U-shaped" structure (shown in Fig. 1(a)). The paper-based sensor (13 × 2 cm) consisted of two ends with one end having a counter electrode (geometric area 8.8 cm^2) that was separated by 0.2 cm from the reference electrode (geometric area 1.5 cm^2), and the other end having a working electrode (geometric area 0.24 cm^2). Wax lines (width 0.5 cm) were printed at both ends to define the reaction and isolating zones. This design enables only the working electrode end of the paper strip to be immersed into the solution for chemical modification (cysteine) and analyte accumulation (copper) but when electrochemical analysis is necessary the sensor strip can be bent to form a "U-shaped" design to have all three electrodes immersed into the electrochemical solution (Fig. 1(b)).

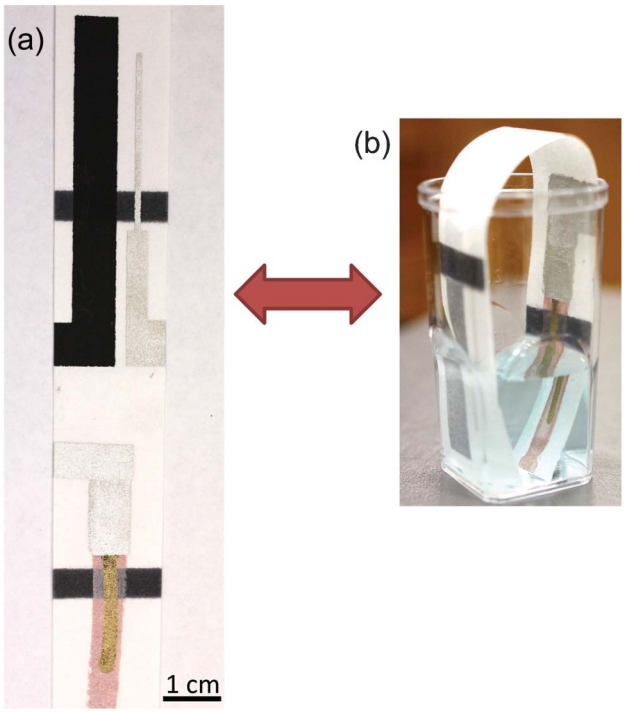

Fig. 1 Paper-based electrochemical sensor with carbon as the counter electrode, silver/silver chloride as the reference electrode and sintered gold nanoparticles as the working electrode. The working electrodes were constructed by coating the filter paper with a thin layer of nail polish, followed by application of gold nanoparticles and flash sintering of the particles. Two horizontal wax lines on either end of the paper are also present to isolate the electrical connections from solution. (a) Paper-based electrochemical sensor in its unbent form to allow the working electrode to be immersed in solution independently of the counter and reference electrodes. (b) Paper-based electrochemical sensor in its U-shaped form to allow the working, counter and reference electrodes to be all immersed in solution for the electrochemical measurement. (Blue dye was added to the solution for visualisation purposes.)

The counter and reference electrodes were fabricated prior to the working electrode. These two electrodes were formed using standard screen-printing techniques on wax patterned filter paper, using carbon ink for the counter electrode and silver/silver chloride ink for the reference electrode. The design of the electrodes was made using Adobe Photoshop 6 software. The counter electrode was screen-printed first prior to screen printing the reference electrode. After each screen-printing step, curing of the electrode ink was allowed to occur by placing the paper in the oven at 80 °C for 15 min.

Gold nanoparticles were deposited using a calligraphy pen to form the working electrode. First, the paper region in which the gold electrode track was to be formed was coated with nail polish. The nail polish coating prevents dispersion of the individual particles in the fibre matrix and allows a dense gold nanoparticle film to be formed. The nail polish drying process typically took less than a few minutes. Following application of the nail polish, ~20 μL 1.0% w/v DMAP–gold nanoparticles in 50% v/v ethanol was applied with a calligraphy pen to the nail polish-coated region of the filter paper.

The paper was then transferred to a hot plate (80 °C) until the solvent had evaporated and the gold nanoparticle film appeared golden (typical geometric area of 0.24 cm^2). A camera flash lamp (Canon Speedlite 550 EX with Fresnel lens removed) was used to sinter the nanoparticles by placing the camera flash unit between 0.9 and 1.4 cm away from the gold nanoparticle film. The flashing (at 24 mm zoom, manual mode, flash output setting of 1/2) was performed twice (30 s apart), upon which a significant decrease in the electrical resistance of the film was observed. The energy was determined using an ultrafast photodiode (UPD-500-UD, ALPHALAS GmbH, Germany) with a spectral range of 190–1100 nm.

For the formation of a cysteine monolayer on gold, the end of the paper strip comprising the sintered gold electrode was immersed in 10 mM L-cysteine in 50 mM ammonium acetate buffer (pH 7.0) for 1 h. The paper working electrode was then rinsed with ammonium acetate buffer followed by water prior to testing.

Analytical determination of copper using paper-based sensor modified with cysteine

Electrochemical measurements were performed using cyclic voltammetry and square wave voltammetry using a PARSTAT 2273 Advanced Electrochemical System (Princeton Applied Research, Tennessee, United States). Prior to copper accumulation, cyclic voltammetry and square wave voltammetry of a

freshly prepared cysteine modified-gold electrode was obtained between −0.4 and +0.3 V in 50 mM ammonium acetate buffer (pH 7.0) containing 50 mM NaCl. Cyclic voltammetry was performed at a scan rate of 0.1 V s^{-1} and square wave voltammetry was performed for the reduction process at a pulse amplitude of 0.025 V, a step of 0.004 V and frequency of 50 Hz.

To evaluate the performance of the cysteine modified-sintered gold paper electrodes, the electrodes were immersed in a stirred test solution of Cu^{2+} in 50 mM ammonium acetate buffer (pH 7.0) for 10 min. After accumulation, followed by rinsing with copper-free ammonium acetate buffer, electrochemical measurements were performed in copper-free ammonium acetate buffer (pH 7.0) containing 50 mM NaCl using cyclic voltammetry and square wave voltammetry as described previously.

Comparison with standard solid-state sensor

The procedure was similar to that described above except that a standard three-electrode system was used (platinum electrode as counter, silver/silver chloride electrode as reference and gold disk electrode as working).

Electrode cleaning was performed for the standard gold disk electrode prior to chemical modification. Standard gold disk electrodes (geometric area 0.0079 cm^2) were first polished to a mirror-like finish with a 1.0 μm, followed by 0.3 and 0.05 μm alumina slurry on microcloth pads. After removal of trace alumina from the surface by rinsing with Milli-Q water and brief cleaning in an ultrasonic bath (~5 min), the electrodes were further cleaned by electrochemically cycling between −0.3 and +1.5 V in 50 mM H_2SO_4 at a scan rate of 0.1 V s^{-1} until a reproducible voltammogram was obtained (typically 20 cycles).

Similar procedures for cysteine modification and copper accumulation were followed as for the paper-based sensor. However, the potential range was shifted positively by 100 mV due to a difference in the composition of silver/silver chloride. Thus, the cyclic voltammetry and square wave voltammetry for the standard sensor were scanned between −0.3 and +0.4 V. After the measurement, the cysteine-modified electrodes were regenerated by the removal of copper. Copper was removed by cyclic voltammetry in 10 mM EDTA, 50 mM ammonium acetate (pH 7.0) and 50 mM NaCl solution. The repeated cycling was run until the reduction–oxidation peaks of copper had disappeared.

Characterisation of electrode surfaces

The cyclic voltammetry at the gold surface (paper and standard electrode) was carried out in a solution containing 2 mM $K_3Fe(CN)_6$ in 1 M sodium nitrate between −0.3 V and +0.7 V at a scan rate of 0.1 V s^{-1}. The potential difference between the cathodic and anodic peaks was used to assess the cleanliness of the gold surface. Different flashing distances (0.9 to 1.4 cm) were investigated for the sintered gold paper surface. The effectiveness of flashing was also probed by modifying the surface with cysteine and testing its copper performance.

In order to investigate the ability of the camera flash sintering technique in removing the DMAP molecule on the gold nanoparticles, Raman measurements of the gold nanoparticle film on paper before and after flash sintering was performed using a Renishaw inVia Raman Microscopy System equipped with an 830 nm diode laser (Renishaw Plc., United Kingdom). Scanning electron microscopy (FEI Nova NanoSEM 230, Oregon, United States) of the gold nanoparticle film before and after flash sintering was also performed to assess the surface topography.

The electrochemical roughness of the sintered gold paper electrode and standard gold disk electrodes were compared using electrochemical impedance spectroscopy. A pair of identical gold electrodes was used and the impedance measurements were recorded between 1 Hz and 1 MHz with an AC amplitude of 50 mV in 1 M sodium nitrate solution, using a PARSTAT 2273 Advanced Electrochemical System. Reductive desorption was performed to determine the amount of cysteine molecules adsorbed on the gold surface. Cyclic voltammetry was carried out in a deoxygenated 0.1 M KOH solution between +0.2 V to −1.2 V at a scan rate of 0.1 V s^{-1}.

Electrochemical area determination

Instead of using the geometrical area of the gold surface, the electrochemical surface area was used. Cyclic voltammograms were performed at the gold electrode between −0.3 to +0.7 V at a scan rate of 0.1 V s^{-1} for 10 cycles in 2 mM $K_3Fe(CN)_6$ and 1 M sodium nitrate. The relationship between the peak current, I_p, and the electrochemical area, A (cm^2), is governed by the Randles-Sevcik relationship:

$$I_p = k\, n^{3/2}\, A\, D^{1/2}\, C^b\, v^{1/2} \quad (1)$$

where k is 2.72 × 10^5, n is the number of electrons transferred per mole of electroactive species, D is the diffusion coefficient (7.6 × 10^{-10} cm^2 s^{-1} for ferricyanide[57]), C^b is the solution concentration in mol L^{-1} and v is the scan rate in V s^{-1}.

For the standard gold disk electrodes used in this work, the electrochemical area was determined to be 0.00579 cm^2 (s = 0.00022 cm^2, n = 9 electrodes) while for the sintered gold paper electrodes this was 0.136 cm^2 (s = 0.017 cm^2, n = 20 electrodes).

Results and discussion

Camera flash sintering of gold nanoparticles

The use of gold nanoparticle inks to fabricate conductive gold electrodes is highly desirable as gold nanoparticles can be easily synthesised and require only a thin coating on the substrate. Direct writing of gold nanoparticles (20 μL) using a calligraphy pen was used to form the thin film of gold nanoparticles on nail polish-coated filter paper. Other methods investigated for depositing the gold nanoparticles included inkjet printing and drop casting in a mould. However, in order to create a conducting gold film using inkjet printing, it required printing six layers of gold nanoparticle ink, which consumed a large volume of ink. Moreover, the drying process in between successive printing layers was time inefficient. Similarly, for drop casting in a mould, a large quantity of ink (80 μL) was needed to completely fill the mould to fabricate a strip of gold film,

and the formation of voids and cracks after drying prevented the formation of a conducting gold electrode.

The gold nanoparticles used in this particular study are stabilised with DMAP molecules. In order to convert the highly resistive gold nanoparticle film to a conductive gold track the DMAP stabilising agent must be removed. Initially, the resistance of the nanoparticle film along the length of the electrode track (0.4 cm) was 15–25 MΩ, whereas upon subjecting the gold nanoparticle film to two pulses of light from a camera flash unit, there was a significant drop in the resistance to less than 50 Ω. This is a positive indication that the majority of DMAP molecules had been removed and that a continuous conducting gold electrode had formed as the necking connections became denser. Since the DMAP had been removed from the surface, the gold nanoparticle cores were no longer protected, and this resulted in coalescence of adjacent gold nanoparticles. Subsequent flashes did not reduce the resistance further, which could be due to the fact that denser neck junctions among the nanoparticles had already been formed with the preceding flash and the grain size of the particles had reached a maximum.[48,49] A concentration of 1.0% w/v DMAP–gold nanoparticles was chosen for the deposition since this amount was sufficient to produce a thin conducting film. When a higher concentration of gold nanoparticle ink (2% w/v) was used, the hydrophilic ink did not spread well on the hydrophobic nail-polish coated surface and thus the sintering of the gold nanoparticle film was less effective (in the kΩ to MΩ range). For lower concentrations (0.5% w/v), the appearance of the gold nanoparticle film was dull and the conductivity remained in the kΩ to MΩ range. This could be due to poor interconnection resulting from a lower density of gold nanoparticles on the surface. So under the optimum conditions of 1.0% w/v DMAP–gold nanoparticles with a deposition volume of 20 μL, this equated to 0.2 mg gold nanoparticles being applied to a single paper sensor. Further evidence for the removal of the DMAP coating from the nanoparticles was *via* dispersibility testing in water and Raman spectroscopy. As the original DMAP–gold nanoparticle ink is water dispersible, the deposited gold nanoparticle film prior to camera flashing also dispersed in water. Following the camera flashing step, the gold nanoparticle film was indispersible in water suggesting that the nanoparticles had sintered to form a metallic structure. Moreover, the Raman spectrum of a freshly applied gold nanoparticle film on paper showed the characteristic peaks of DMAP prior to flash sintering (Fig. 2) which were absent in the Raman spectrum after flashing the gold nanoparticle film twice at a distance of 1.1 cm. The strong vibration at 751 cm^{-1} for the DMAP crystal and at 761 cm^{-1} for the DMAP–gold nanoparticle film can be assigned to C–N–C wagging, whereas the vibration at 950 cm^{-1} for the DMAP crystal and at 948 cm^{-1} for the DMAP–gold nanoparticle film can be assigned to ring breathing, CH_3 rocking and C–H out-of-plane bending.[58] For other vibrational assignments refer to the supplementary section.†

As the removal of DMAP molecules surrounding the gold nanoparticles depends on the energy of the camera flash unit (refer to the supplementary section†), this process was optimised by varying the flashing distance. The distance between the camera flash unit and the paper substrate was varied between 0.9–1.4 cm and was subjected to two pulses of light from the camera flash unit. In all cases, the electrical resistance decreased from 15–25 MΩ to less than 50 Ω. However, visually for the flashing distance of 0.9 cm, the bulk of the gold nanoparticles appeared at the periphery of the electrode track. Further investigations were carried out by assessing the electrochemical performance of the sintered gold paper electrodes in ferricyanide solution. Fig. 3 shows that the ferricyanide peak separation can be modulated with flashing distance and they ranged between 120 and 170 mV for 0.9 to 1.4 cm flashing distance. At a flashing distance of 1.1 cm, the smallest peak separation was obtained indicating a more continuous gold film and a surface more free from organic contaminants than at other flashing distances. Larger peak separations from flashing distances greater than 1.1 cm could be due to the insufficiency of heat generated at the gold nanoparticles, whereas at flashing distances less than 1.1 cm overheating of the gold nanoparticles and migration of the

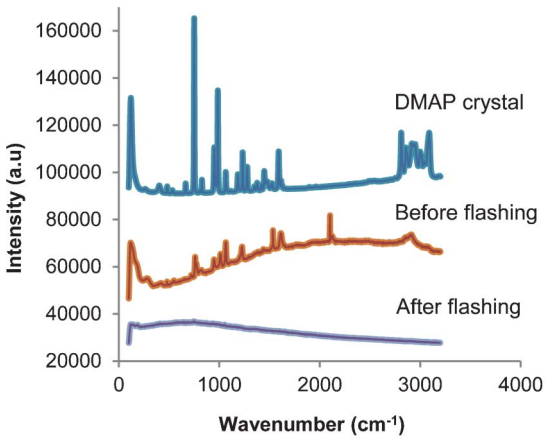

Fig. 2 Raman spectra of DMAP–gold nanoparticle film electrodes before and after flashing twice at a distance of 1.1 cm. Flash sintering of the gold nanoparticles resulted in the absence of a DMAP Raman signature. For reference, the Raman spectrum of a DMAP crystal is shown.

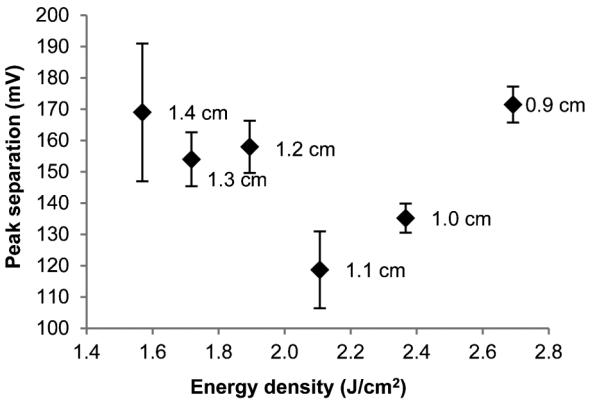

Fig. 3 Separation between the anodic and cathodic peaks of the ferricyanide/ferrocyanide redox couple as a function of energy density obtained by varying the flashing distance between the gold nanoparticle film and the camera flash unit. The data label is the flashing distance.

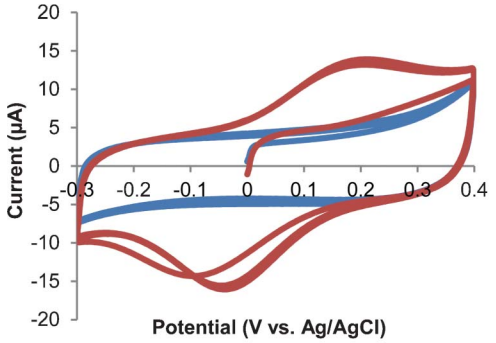

Fig. 4 Cyclic voltammograms at a cysteine-modified sintered gold nanoparticle film paper electrode (1.1 cm flashing distance) measured in 50 mM ammonium acetate (pH 7.0) and 50 mM NaCl before accumulation of copper ions (blue curve) and after accumulation in 280 ppb copper for 10 min (red curve). Scan rate was 0.1 V s^{-1}. Multiple cycles in the voltammogram illustrate stable electrochemistry.

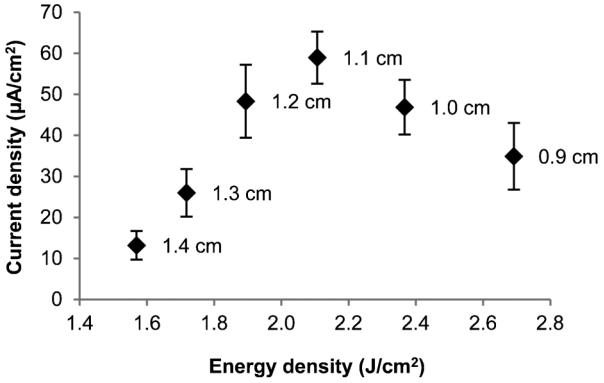

Fig. 5 Copper current density obtained using square wave voltammetry at cysteine-modified sintered gold paper electrodes as a function of energy density. The electrodes were accumulated in 280 ppb copper solution for 10 min. The energy was varied by flashing the nanoparticles at different distances as shown in the data label.

particles towards the periphery of the electrode track resulted. In comparison, a standard gold disk electrode that had been mechanically polished and electrochemically cleaned in H_2SO_4 resulted in a ferricyanide peak separation of 80–90 mV.[59] Due to the surface roughness of the sintered gold nanoparticle electrodes, it is reasonable to expect these electrodes to exhibit a higher peak separation than a standard gold disk electrode.

Analytical determination of copper using cysteine-modified gold nanoparticle film

To demonstrate that the sintered gold nanoparticle film on paper is a viable alternative to solid-state gold as a working electrode, it is necessary that the same type of surface chemistries can be applied. As SAMs of thiols on gold are widely explored, the formation of cysteine on the sintered gold paper electrode and its ability to chelate to copper ions was evaluated. Fig. 4 shows the cyclic voltammograms at a cysteine-modified sintered gold nanoparticle film paper electrode before and after the accumulation of copper ions. Prior to copper accumulation there were no copper redox peaks in the voltammogram as expected. After Cu^{2+} ions (280 ppb) had been accumulated at the cysteine modified surface at open circuit potential for 10 min, and measured in copper-free ammonium acetate buffer, the appearance of redox peaks at E_a = 0.185 V and E_c = −0.037 V (Fig. 4) were observed, which were stable over several cycles in the voltammogram. The redox peaks can be ascribed to Cu^{2+}/Cu^0 where Cu^{2+} ions are captured by cysteine in solution and are underpotentially deposited as Cu^0 upon reduction, and subsequently reoxidised back to Cu^{2+}.[23] For quantification purposes, square wave voltammetry was used as it offers a more sensitive technique than cyclic voltammetry. A Cu^{2+} peak current of 13 μA was obtained after accumulation in 280 ppb Cu^{2+} for 10 min (refer to the supplementary section†). Without self-assembly of cysteine on the sintered gold nanoparticle paper electrode, the square wave voltammogram revealed a small copper response (2.0 μA) at a more positive potential of +0.20 V after 280 ppb copper accumulation. This indicates that for the modified gold electrode, the cysteine molecule is largely responsible for the copper binding interaction.

Further studies on the effect of flashing distance were performed by evaluating the reductive copper peak current obtained from square wave voltammetry. The cysteine-modified sintered gold nanoparticle paper electrode with 1.1 cm flashing distance gave a higher copper current density compared to the other samples prepared by flashing the gold nanoparticles films at a different distance (Fig. 5). This result is not surprising considering that the 1.1 cm flashing distance also gave the smallest ferricyanide peak separation for the sintered gold nanoparticle film. This further justifies that the 1.1 cm flashing distance provides an optimal surface to allow more efficient formation of cysteine molecules on the gold paper electrode.

Since the copper peak current is dependent on the concentration of copper ions in the accumulation solution, this can be applied to the quantification of different levels of copper.

The peak current density dependence from square wave voltammetry as a function of copper concentration was determined upon accumulation in copper ion solution for 10 min in ammonium acetate buffer (pH 7.0). For the cysteine-modified sintered gold nanoparticle paper electrodes, detectable levels of copper spanned 3 orders of magnitude with a limit of detection of 50 ppb (Fig. 6).

To assess whether the sintered gold nanoparticle paper electrode is a viable alternative to the standard gold disk working electrode, the copper performance of these electrodes upon cysteine modification was compared. The standard gold disk electrodes were also able to determine copper concentrations spanning 3 orders of magnitude, albeit at lower concentrations, with a limit of detection of 5 ppb. Despite the lower sensing ability of the paper-based sensor, the result is highly encouraging considering that the reported values are normalised to the electrochemical area of the electrodes due to different electrodes having slightly different areas. If the working electrode area of the sensors was increased, then in

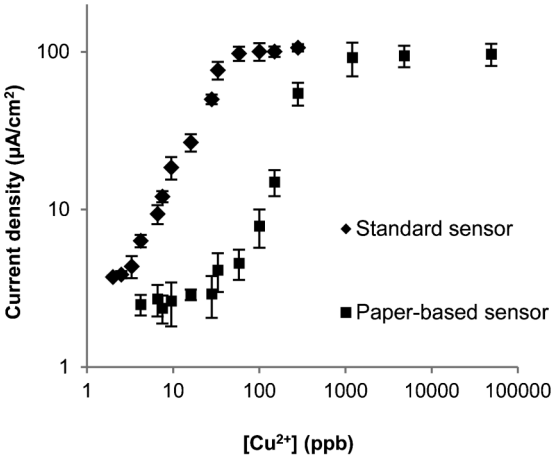

Fig. 6 Calibration curve of peak current density *versus* Cu^{2+} concentration obtained from square wave voltammetry. Copper ions were accumulated at the cysteine-modified gold electrodes for 10 min. The error bars are the standard deviation of at least four repeated measurements using different electrodes.

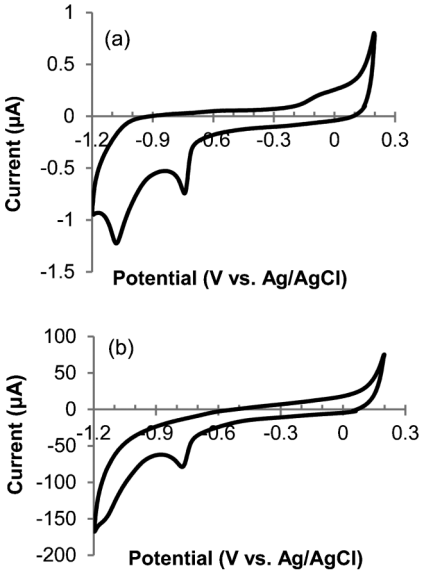

Fig. 7 Cyclic voltammograms from +0.2 to −1.2 V of the reductive desorption of cysteine from a (a) standard gold disk electrode and (b) sintered gold nanoparticle film paper electrode in deoxygenated 0.1 M KOH solution. Scan rate of 0.1 V s^{-1}.

principle, this should improve the copper detection limit as the number of cysteine molecules available for copper binding on the surface would have also increased. Increasing the working electrode area of a gold disk electrode is expensive but for the paper-based sensors this can be easily achieved by coating the gold nanoparticles over a larger surface area. As the total amount of gold nanoparticles utilised would still be small, this is a viable low-cost option to improving the sensitivity.

The difference in performance between the two types of gold electrodes could be attributed to a number of factors: surface coverage of cysteine as well as the porosity and roughness of the gold. A lower surface coverage of cysteine for the sintered gold nanoparticle paper electrode would imply a smaller number of cysteine sites available for copper binding whereas if the surface was porous and rough, this may result in some of the cysteine being less accessible to copper ions. Either of these factors could shift the thermodynamic binding K_a to a lower value. As the formation of a stable tetrahedral metal complex relies on the binding of two cysteine molecules to Cu^{2+} (eqn (2)), the K_a values (eqn (3)) for the paper-based sensors and standard sensors were determined to be 100 ppm^{-2} and 11 000 ppm^{-2}, respectively.

$$Cu^{2+} + 2\ Cys \rightleftharpoons Cys - Cu^{2+} - Cys \quad (2)$$

$$K_a = \frac{[Cys - Cu^{2+} - Cys]}{[Cys]^2[Cu^{2+}]} \quad (3)$$

Reductive desorption of cysteine and surface morphology of gold electrodes

The surface coverage of cysteine on the electrodes was evaluated by reductive desorption of the cysteine SAM from the gold surface by sweeping the potential of the working electrode negatively in deoxygenated 0.1 M KOH solution from +0.2 V to −1.2 V at 0.1 V s^{-1}. Two desorption peaks were observed at −0.780 and −1.070 V (Fig. 7(a)), which could arise from cleavage of the gold–sulfur bond,[60] rearrangement of the thiol after cleavage,[24] or the existence of various surface domains on gold.[61,62] We used both peaks to take into account the surface coverage of cysteine on a standard gold disk working electrode and calculated a value of 0.470 nmol cm^{-2} (s = 0.070 nmol cm^{-2}, n = 6 electrodes). This result is slightly lower than the ideal coverage of 0.760 nmol cm^{-2} expected for a $(\sqrt{3} \times \sqrt{3})R30^\circ$ overlayer structure of alkanethiols on Au(111).[24,63]

For the sintered gold nanoparticle film paper substrates, a cysteine desorption peak at −0.760 V and a less pronounced peak at −1.120 V *vs.* standard Ag/AgCl (Fig. 7(b)) was observed. The surface coverage of the cysteine SAM was 0.877 nmol cm^{-2} (s = 0.091 nmol cm^{-2}, n = 4 electrodes). This value is larger than what would be expected for a monolayer. As the evaluation of the cysteine coverage cannot equate to multi-layers, this result suggests that the method of determination of the surface area underestimates the true surface area of the electrodes on paper. Moreover, the slope between −1.0 to −0.2 V in the reverse sweep of the voltammogram (Fig. 7(b)), which was absent at the standard gold disk electrode, suggests a conductive element associated with a rough surface or porous electrode.

As a result of the hypothesis that the electrodes may be very rough, the morphology of the sintered gold paper electrode and the standard gold disk electrode was assessed through electrochemical impedance spectroscopy to measure and compare the roughness of the two. The impedance Z can be described by:

$$Z = (j\omega C)^{-\alpha} \quad (4)$$

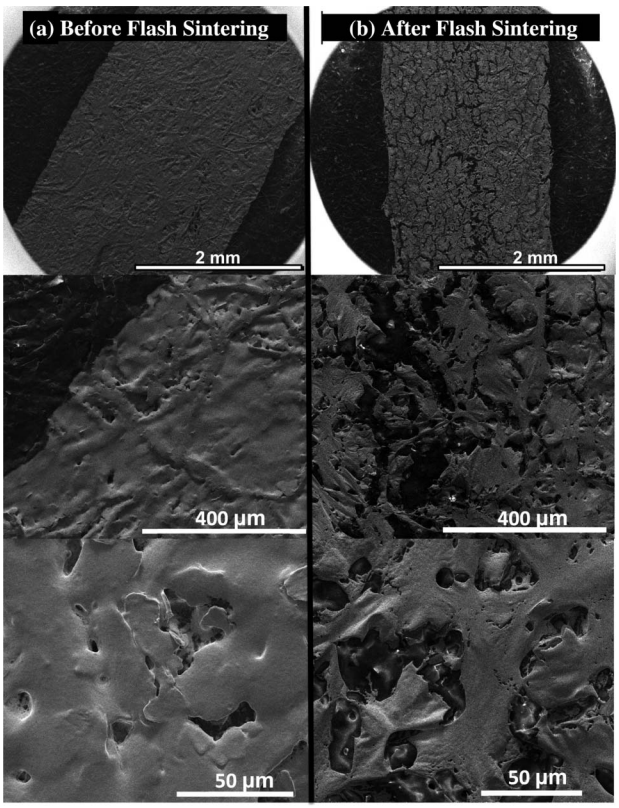

Fig. 8 Scanning electron microscopy images of the gold nanoparticle film on nail polish-coated paper before (a) and after (b) camera flash sintering.

where j is an imaginary number, ω is the angular frequency, C is the capacitance and α is the constant phase element.[64] The α value provides an indication of the surface heterogeneity and was determined for the standard solid-state gold disk electrode and sintered gold nanoparticle paper electrode to be 0.87 and 0.71, respectively. The smaller α value measured for the sintered gold paper electrode implies greater heterogeneity of the surface compared to the standard gold electrode.

Scanning electron microscopy images in Fig. 8(a) of the gold nanoparticle film before camera flashing show that the structure of the film follows the alignment of the fibre paper matrix. The presence of some cracks and voids were observed, which were even more pronounced after the sintering process Fig. 8(b). We attribute these cracks and defects to the large volume reduction of the gold nanoparticle film during the sintering process, which leads to the formation of a denser structure.[42,46,65]

The reductive desorption, electrochemical impedance and scanning electron microscopy characterisation studies support that the morphology of the gold surface on the paper-based electrochemical sensor plays a large influence on the sensing performance. The presence of cracks and voids on the sintered gold nanoparticle film paper electrode could explain the weaker performance of the paper-based sensor in detecting copper.

Conclusions

The formation of gold electrodes on paper could provide a suitable alternative for carbon-based paper electrodes by offering ease in surface functionalisation. We have demonstrated the utility of sintered gold nanoparticle films as a sensing surface in paper-based electrochemical sensors through the use of DMAP-coated gold nanoparticles. The gold nanoparticle film could be made highly conductive through camera flash sintering of the nanoparticles and we have shown that it is possible to form self-assembled monolayers of thiols on the gold surface. This provided a platform for sensing whereby a cysteine-modified gold surface was used to detect copper ions electrochemically. Considering the volume requirements of gold nanoparticles and the simplicity in processing, sintered gold nanoparticle films on paper can potentially form a basis for low-cost, disposable analysis of chemically and biologically relevant species in the future.

Acknowledgements

We would like to thank J. Myers for her help in preparing the gold nanoparticles.

References

1 W. A. Zhao and A. Van den Berg, *Lab Chip*, 2008, **8**, 1988–1991.
2 D. L. Clegg, *Anal. Chem.*, 1950, **22**, 48–59.
3 W. Dungchai, O. Chailapakul and C. S. Henry, *Analyst*, 2011, **136**, 77–82.
4 S. M. Z. Hossain, R. E. Luckham, M. J. McFadden and J. D. Brennan, *Anal. Chem.*, 2009, **81**, 9055–9064.
5 A. W. Martinez, S. T. Phillips, G. M. Whitesides and E. Carrilho, *Anal. Chem.*, 2010, **82**, 3–10.
6 A. W. Martinez, S. T. Phillips, M. J. Butte and G. M. Whitesides, *Angew. Chem., Int. Ed.*, 2007, **46**, 1318–1320.
7 A. W. Martinez, S. T. Phillips, E. Carrilho, S. W. Thomas, H. Sindi and G. M. Whitesides, *Anal. Chem.*, 2008, **80**, 3699–3707.
8 D. D. Liana, B. Raguse, J. J. Gooding and E. Chow, *Sensors*, 2012, **12**, 11505–11526.
9 W. Dungchai, O. Chailapakul and C. S. Henry, *Anal. Chem.*, 2009, **81**, 5821–5826.
10 K. Abe, K. Suzuki and D. Citterio, *Anal. Chem.*, 2008, **80**, 6928–6934.
11 X. Li, J. F. Tian, T. Nguyen and W. Shen, *Anal. Chem.*, 2008, **80**, 9131–9134.
12 W. Wang, W. Y. Wu, W. Wang and J. J. Zhu, *J. Chromatogr., A*, 2010, **1217**, 3896–3899.
13 L. Ge, S. Wang, X. Song, S. Ge and J. Yu, *Lab Chip*, 2012, **12**, 3150–3158.
14 A. Govindarajan, S. Ramachandran, G. Vigil, P. Yager and K. Böhringer, *Lab Chip*, 2012, **12**, 174–181.
15 H. Liu, Y. Xiang, Y. Lu and R. M. Crooks, *Angew. Chem.*, 2012, **124**, 7031–7034.

16 A. Apilux, W. Dungchai, W. Siangproh, N. Praphairaksit, C. S. Henry and O. Chailapakul, *Anal. Chem.*, 2010, **82**, 1727–1732.
17 Z. H. Nie, C. A. Nijhuis, J. L. Gong, X. Chen, A. Kumachev, A. W. Martinez, M. Narovlyansky and G. M. Whitesides, *Lab Chip*, 2010, **10**, 477–483.
18 J. Lankelma, Z. Nie, E. Carrilho and G. M. Whitesides, *Anal. Chem.*, 2012, **84**, 4147–4152.
19 Z. H. Nie, F. Deiss, X. Y. Liu, O. Akbulut and G. M. Whitesides, *Lab Chip*, 2010, **10**, 3163–3169.
20 T. Wink, S. Van Zuilen, A. Bult and W. Van Bennekom, *Analyst*, 1997, **122**, 43R–50R.
21 J. J. Gooding, F. Mearns, W. Yang and J. Liu, *Electroanalysis*, 2003, **15**, 81–96.
22 A. Ulman, *Chem. Rev.*, 1996, **96**, 1533.
23 E. Chow, E. L. S. Wong, T. Böcking, Q. T. Nguyen, D. B. Hibbert and J. J. Gooding, *Sens. Actuators, B*, 2005, **111**, 540–548.
24 W. Yang, J. J. Gooding and D. B. Hibbert, *J. Electroanal. Chem.*, 2001, **516**, 10–16.
25 A. C. Liu, D. Chen, C. C. Lin, H. H. Chou and C. Chen, *Anal. Chem.*, 1999, **71**, 1549–1552.
26 S. Flink, B. A. Boukamp, A. van den Berg, F. C. J. M. van Veggel and D. N. Reinhoudt, *J. Am. Chem. Soc.*, 1998, **120**, 4652–4657.
27 J. J. Gooding and D. B. Hibbert, *TrAC, Trends Anal. Chem.*, 1999, **18**, 525–533.
28 J. J. Gooding, P. Erokhin and D. B. Hibbert, *Biosens. Bioelectron.*, 2000, **15**, 229–239.
29 D. Losic, J. J. Gooding, J. Shapter, D. Hibbert and K. Short, *Electroanalysis*, 2001, **13**, 1385–1393.
30 I. Willner, M. Lion-Dagan, S. Marx-Tibbon and E. Katz, *J. Am. Chem. Soc.*, 1995, **117**, 6581–6592.
31 J. Gooding, V. Praig and E. Hall, *Anal. Chem.*, 1998, **70**, 2396–2402.
32 T. Lötzbeyer, W. Schuhmann and H. L. Schmidt, *Sens. Actuators, B*, 1996, **33**, 50–54.
33 F. Patolsky, M. Zayats, E. Katz and I. Willner, *Anal. Chem.*, 1999, **71**, 3171–3180.
34 K. Kerman, D. Ozkan, P. Kara, B. Meric, J. J. Gooding and M. Ozsoz, *Anal. Chim. Acta*, 2002, **462**, 39–47.
35 E. L. S. Wong, E. Chow and J. J. Gooding, *Langmuir*, 2005, **21**, 6957–6965.
36 E. L. S. Wong and J. J. Gooding, *Anal. Chem.*, 2006, **78**, 2138–2144.
37 J. Liu, M. J. Casavant, M. Cox, D. Walters, P. Boul, W. Lu, A. Rimberg, K. Smith, D. T. Colbert and R. E. Smalley, *Chem. Phys. Lett.*, 1999, **303**, 125–129.
38 X. Nan, Z. Gu and Z. Liu, *J. Colloid Interface Sci.*, 2002, **245**, 311–318.
39 R. M. Crooks, M. Zhao, L. Sun, V. Chechik and L. K. Yeung, *Acc. Chem. Res.*, 2001, **34**, 181–190.
40 H. C. Yoon, M. Y. Hong and H. S. Kim, *Anal. Biochem.*, 2000, **282**, 121–128.
41 M. Brust, M. Walker, D. Bethell, D. J. Schiffrin and R. Whyman, *J. Chem. Soc., Chem. Commun.*, 1994, 801–802.
42 J. Perelaer, B. J. D. Gans and U. S. Schubert, *Adv. Mater.*, 2006, **18**, 2101–2104.
43 M. Hummelgård, R. Zhang, H. E. Nilsson and H. Olin, *PLoS One*, 2011, **6**, e17209.
44 M. L. Allen, M. Aronniemi and T. Mattila, *Nanotechnology*, 2008, **19**, 175201–175205.
45 S. H. Ko, H. Pan, C. P. Grigoropoulos, C. K. Luscombe, J. M. J. Fréchet and D. Poulikakos, *Nanotechnology*, 2007, **18**, 345202.
46 D. Tobjörk, H. Aarnio, P. Pulkkinen, R. Bollström, A. Määttänen, P. Ihalainen, T. Mäkelä, J. Peltonen, M. Toivakka and H. Tenhu, *Thin Solid Films*, 2012, **520**, 2949–2955.
47 R. Abbel, T. van Lammeren, R. Hendriks, J. Ploegmakers, E. J. Rubingh, E. R. Meinders and W. A. Groen, *MRS Commun.*, 2012, **2**, 145–150.
48 K. Yung, X. Gu, C. Lee and H. Choy, *J. Mater. Process. Technol.*, 2010, **210**, 2268–2272.
49 W. H. Chung, H. J. Hwang, S. H. Lee and H. S. Kim, *Nanotechnology*, 2013, **24**, 035202.
50 H. J. Hwang, W. H. Chung and H. S. Kim, *Nanotechnology*, 2012, **23**, 485205.
51 S. H. Park, S. Jang, D. J. Lee, J. Oh and H. S. Kim, *J. Micromech. Microeng.*, 2013, **23**, 015013.
52 H. S. Kim, S. R. Dhage, D. E. Shim and H. T. Hahn, *Appl. Phys. A: Mater. Sci. Process.*, 2009, **97**, 791–798.
53 B. Raguse, G. Baxter and L. Wieczorek, *Personal Communication.*
54 D. I. Gittins and F. Caruso, *Angew. Chem., Int. Ed.*, 2001, **40**, 3001–3004.
55 E. Carrilho, A. W. Martinez and G. M. Whitesides, *Anal. Chem.*, 2009, **81**, 7091–7095.
56 Y. Lu, W. Shi, J. Qin and B. Lin, *Anal. Chem.*, 2010, **82**, 329–335.
57 S. Petrovic, *Chem. Educ.*, 2000, **5**, 231–235.
58 N. Sundaraganesan, S. Kalaichelvan, C. Meganathan, B. D. Joshua and J. Cornard, *Spectrochim. Acta, Part A*, 2008, **71**, 898–906.
59 L. M. Fischer, M. Tenje, A. R. Heiskanen, N. Masuda, J. Castillo, A. Bentien, J. Émneus, M. H. Jakobsen and A. Boisen, *Microelectron. Eng.*, 2009, **86**, 1282–1285.
60 R. F. Carvalhal, R. Sanches Freire and L. T. Kubota, *Electroanalysis*, 2005, **17**, 1251–1259.
61 M. M. Walczak, D. D. Popenoe, R. S. Deinhammer, B. D. Lamp, C. Chung and M. D. Porter, *Langmuir*, 1991, **7**, 2687–2693.
62 D. E. Weisshaar, B. D. Lamp and M. D. Porter, *J. Am. Chem. Soc.*, 1992, **114**, 5860–5862.
63 M. S. El-Deab and T. Ohsaka, *Electrochim. Acta*, 2004, **49**, 2189–2194.
64 B. Hirschorn, M. E. Orazem, B. Tribollet, V. Vivier, I. Frateur and M. Musiani, *J. Electrochem. Soc.*, 2010, **157**, C452–C457.
65 D. J. Lee, J. H. Oh and H. S. Bae, *Mater. Lett.*, 2010, **64**, 1069–1072.